HHS Public Access

Author manuscript

Science. Author manuscript; available in PMC 2022 April 14.

Published in final edited form as:

Science. 2021 April 23; 372(6540): . doi:10.1126/science.aba2374.

Preventing *Engrailed-1* activation in fibroblasts yields wound regeneration without scarring

Shamik Mascharak[1,2], **Heather E. des Jardins-Park**[1,2], **Michael F. Davitt**[1], **Michelle Griffin**[1], **Mimi R. Borrelli**[1], **Alessandra L. Moore**[1], **Kellen Chen**[1], **Bryan Duoto**[1], **Malini Chinta**[1], **Deshka S. Foster**[1], **Abra H. Shen**[1], **Michael Januszyk**[1], **Sun Hyung Kwon**[1], **Gerlinde Wernig**[2,3], **Derrick C. Wan**[1], **H. Peter Lorenz**[1], **Geoffrey C. Gurtner**[1,*], **Michael T. Longaker**[1,2,*]

[1]Department of Surgery, Division of Plastic and Reconstructive Surgery, Stanford University School of Medicine, Stanford, CA 94305, USA.

[2]Institute for Stem Cell Biology and Regenerative Medicine, Stanford University School of Medicine, Stanford, CA 94305, USA.

[3]Department of Pathology, Stanford University School of Medicine, Stanford, CA 94305, USA.

Abstract

Skin scarring, the end result of adult wound healing, is detrimental to tissue form and function. *Engrailed-1* lineage–positive fibroblasts (EPFs) are known to function in scarring, but *Engrailed-1* lineage–negative fibroblasts (ENFs) remain poorly characterized. Using cell transplantation and transgenic mouse models, we identified a dermal ENF subpopulation that gives rise to postnatally derived EPFs by activating *Engrailed-1* expression during adult wound healing. By studying ENF responses to substrate mechanics, we found that mechanical tension drives *Engrailed-1* activation via canonical mechanotransduction signaling. Finally, we showed that blocking mechanotransduction signaling with either verteporfin, an inhibitor of Yes-associated protein (YAP), or fibroblast-specific transgenic YAP knockout prevents *Engrailed-1* activation and promotes wound regeneration by ENFs, with recovery of skin appendages, ultrastructure, and mechanical strength. This finding suggests that there are two possible outcomes to postnatal wound healing: a fibrotic response (EPF-mediated) and a regenerative response (ENF-mediated).

As a part of the wound-healing process, adult skin generally develops fibrotic scar tissue. Scars differ from normal skin in that they lack dermal appendages (hair follicles, glands,

*Corresponding author: longaker@stanford.edu (M.T.L.); ggurtner@stanford.edu (G.C.G.).

Author contributions: S.M. conceived, designed, and oversaw the experiments, with suggestions from H.E.dJ.-P, M.R.B., A.L.M., and M.T.L.; S.M., H.E.dJ.-P., M.R.B., A.L.M., M.F.D., M.G., K.C., B.D., M.C., D.S.F., A.H.S., M.J., and S.H.K. performed wounding experiments, prepared specimens and images, and analyzed the data; S.M. and H.E.dJ.-P. wrote the manuscript; and G.W., D.C.W., H.P.L., G.C.G., and M.T.L. edited the manuscript.

Competing interests: The authors declare no competing interests.

SUPPLEMENTARY MATERIALS

science.sciencemag.org/content/372/6540/eaba2374/suppl/DC1

Materials and Methods

Figs. S1 to S13

References (41, 42)

etc.); are characterized by fibrotic extracellular matrix (ECM) with dense, parallel fibers (versus the “basket-weave” pattern that gives skin its flexibility and strength); and, because of this altered fiber structure, are weaker than unwounded skin. Scarring can cause disfigurement, growth restriction, and permanent functional loss (1–5), ultimately costing the US more than $20 billion every year; the cost worldwide is likely much higher (6, 7). A scar-preventing therapy should restore appendages, normal matrix structure, and strength comparable to those of unwounded skin (8, 9). Despite decades of research, wound healing without scarring has not been achieved.

To advance our understanding of scarring and develop new therapies, it is important to identify cell populations associated with scarring. It is generally believed that fibroblasts, which synthesize and organize ECM, are key mediators of scarring. Previously, we reported that the dorsal mouse dermis contains at least two distinct fibroblast lineages: *Engrailed-1* (*En1*) lineage–negative fibroblasts (ENFs) and *En1* lineage–positive fibroblasts (EPFs) (10). *En1*-expressing fibroblasts emerge during normal development in utero. These cells and their progeny, termed embryonic *En1*-positive fibroblasts or eEPFs, cease to express *En1* in homeostatic postnatal skin (10). Although EPFs predominate in wounds (10), it is not known whether they are derived from expansion of eEPFs already present in skin or arise de novo by activating *En1* expression in ENFs within wounds (postnatally derived EPFs, pEPFs). Using fibroblast transplantation and genetic tracing to spatiotemporally explore *En1* expression, we have identified an ENF subpopulation that generates pEPFs by activating *En1* expression within wounds. By modulating substrate mechanics in vitro and in vivo, we show that tension drives *En1* activation via canonical mechanotransduction (i.e., YAP) signaling. Finally, we demonstrate that YAP inhibition or genetic knockout blocks *En1* activation in wounds, yielding ENF-mediated regeneration with recovery of secondary skin elements (hair follicles and glands), ECM architecture, and tensile strength indistinguishable from those of unwounded skin. Our findings shed light on the origin of the specific fibroblasts involved in scarring and molecular pathways driving fibrosis, suggesting a therapeutic strategy for wound regeneration.

A fibroblast subpopulation activates *Engrailed-1* in the wound environment

To study defined fibroblast lineages in the wound environment in vivo, we used fluorescence-activated cell sorting (FACS) to isolate ENFs (tdTomato$^+$) and EPFs (GFP$^+$) from $En1^{Cre};R26^{mTmG}$ mouse dorsal skin [in which En1 lineage–positive cells express membrane-bound green fluorescent protein (GFP) and En1 lineage–negative cells express membrane-bound tdTomato; see supplementary materials]. ENFs or EPFs were transplanted into wild-type mouse dorsal dermis, and then the engrafted skin was wounded (Fig. 1A). Once healed [postoperative day (POD) 14], wounds (scars) and surrounding skin were harvested and analyzed histologically. Within unwounded skin, all transplanted fibroblasts demonstrated quiescent, elongated morphology (Fig. 1B, top). Wound-engrafted EPFs exhibited activated morphology with extended cellular processes (Fig. 1B, bottom left), consistent with prior reports of wound EPF phenotype (10). In contrast to ENF-engrafted unwounded skin, which contained only tdTomato$^+$ ENFs (Fig. 1B, top right), ENF-engrafted wounds contained GFP$^+$ cells with activated morphology similar to that of wound-engrafted EPFs (Fig. 1B, bottom right), indicating that transplanted ENFs expressed *En1* (causing Cre-

driven *mT/mG* reporter recombination) to become pEPFs within the wound environment. We previously observed that collagen deposition is unique to EPFs (10); immunostaining for type I collagen (col-I; Fig. 1C) and colocalization analysis in wounds confirmed that pEPFs had significantly greater overlap with col-I than did ENFs that had not activated *En1* expression (Fig. 1D), indicating increased collagen production specifically from *En1*-expressing cells.

Although these results suggested ENF-to-pEPF conversion in wounds, it was possible that a small number of contaminating EPFs had disproportionately proliferated to produce GFP^+ cells observed in ENF-transplanted wounds. Because cells endured several hours of cold ischemia before engraftment, it was also important to confirm that postnatal *En1* activation is specific to the wound setting. We therefore generated $En1^{Cre\text{-}ERT}$;*Ai6* transgenic mice ($En1^{Cre}$ active only after tamoxifen induction) and administered tamoxifen before wounding, so that only cells that activated *En1* expression during wound healing expressed GFP (Fig. 1E; no GFP^+ cells observed without tamoxifen, fig. S1). POD 14 scars and skin were subjected to FACS (fig. S2, A and B) and histologic analysis. Unwounded skin had few GFP^+ cells (Fig. 1F, top left); in healed wounds, ~40% of fibroblasts were GFP^+ (Fig. 1F, bottom left, and fig. S2C; similar GFP^+ fraction with tamoxifen induction initiated at POD 0 rather than 5 days prior, fig. S1). These data corroborated our findings of *En1* activation in wound-engrafted ENFs (Fig. 1B) and suggested that postnatal ENF-to-EPF transition generates a substantial fraction of scar-producing EPFs (Fig. 1G).

ENFs likely represent multiple subpopulations; we therefore questioned whether ENFs corresponding to previously reported, surface marker–defined anatomical subpopulations (11, 12) exhibited differing wound phenotypes, including *En1* activation. We used FACS to sort dorsal dermal fibroblasts (Lin^-; see supplementary materials) from $En1^{Cre}$;*Ai6* mice into EPFs (GFP^+) and ENFs (GFP^-), which were further sorted into papillary dermal ($CD26^+Sca1^-$), reticular dermal ($Dlk1^+Sca1^-$), and hypodermal ($Dlk1^{+/-}Sca1^+$) (11, 12) subfractions (Fig. 1H; FACS strategy, fig. S2, D and E). Similar to prior reports (11), papillary, reticular, and hypodermal fibroblasts constituted 19%, 12%, and 52% of $PDGFR\alpha^+$ ENFs, respectively (fig. S2F, left). When we defined fibroblasts as Lin^- (PDGFRα-agnostic), ENF subpopulations were more evenly distributed (fig. S2F, right). As previously reported, a substantial fraction of ENFs were $PDGFR\alpha^-$ (fig. S2E). We therefore did not include this marker in our sorting strategy.

ENF subfractions underwent engraftment into $R26^{mTmG}$ ($tdTomato^+$) mice and wounding (Fig. 1H). Papillary or hypodermal ENF-engrafted scars lacked GFP^+ cells (Fig. 1I, left and right). However, reticular ENF-engrafted wounds had numerous GFP^+ cells (Fig. 1I, center, white arrowheads), implicating reticular ($Dlk1^+Sca1^-$) ENFs as the primary subpopulation capable of postnatal wound *En1* activation. Consistent with previous reports of Dlk1 as a reticular (deep) dermal fibroblast marker (11, 12), its expression in unwounded skin of tamoxifen-induced $En1^{Cre\text{-}ERT}$;*Ai6* mice was confined to the deep dermis (Fig. 1F, top right). However, in scars, Dlk1 was expressed throughout the dermis (Fig. 1F, bottom). $Dlk1^+$ ENFs were closely associated with chains of pEPFs and overlapping Dlk1/GFP expression (Fig. 1F, bottom right, white arrowheads). Our findings did not explicitly rule out that rare preexisting skin pEPFs proliferated after wounding, but their relative absence

in unwounded skin, vastly greater numbers in scars, and colocalization with wound Dlk1$^+$ ENFs suggest that reticular ENFs expand and activate *En1* after injury to contribute to scarring.

Postnatal *Engrailed-1* activation is mechanoresponsive

Cell surface integrins couple to focal adhesion kinase (FAK) to communicate mechanical environmental cues, ultimately affecting transcription via Rho/Rho-associated protein kinase (ROCK) signaling (13). Mechanotransduction modulates wound-resident cells (14–16), particularly fibroblasts: Increasing wound tension increases fibroblasts' profibrotic gene expression [e.g., collagens, transforming growth factor–β (TGF-β)] (15); offloading wound tension significantly reduces scarring (17).

We hypothesized that mechanical cues activate ENFs to express *En1*, thereby generating fibrotic pEPFs. *En1*^{Cre};*R26*^{mTmG} ENFs were cultured on (i) tissue culture plastic (TCPS; high-stiffness); (ii) TCPS with ROCK inhibitor Y-27632 (blocked stiffness-sensing); or (iii) 3D collagen hydrogels (low-stiffness; Fig. 2A). After 14 days, ENFs activated *En1* expression on TCPS (Fig. 2, B, left, and C, green circles) but largely failed to activate *En1* in soft hydrogel (Fig. 2, B, right, and C, blue triangles) or with mechanotransduction inhibition (Fig. 2, B, center, and C, red squares). We next fractionated *En1*^{Cre};*Ai6* ENF subpopulations (Fig. 1H) and cultured each on TCPS, with or without Y-27632 (Fig. 2D). Papillary and hypodermal ENFs minimally activated *En1* (Fig. 2E, left and right), whereas reticular ENFs showed near-complete conversion to pEPFs after 14 days (Fig. 2E, top center), consistent with in vivo wound findings (Fig. 1I); this conversion was blocked by ROCK inhibitor (Fig. 2E, bottom center). These data suggested that reticular ENFs express *En1* in response to mechanical cues via canonical mechanotransduction pathways (Fig. 2F).

To test whether mechanical stress promoted ENF-to-EPF transition in vivo, we created dorsal incisions in tamoxifen-induced *En1*$^{Cre\text{-}ERT}$;*Ai6* mice; per established protocol (15), we affixed distraction devices over wounds and expanded them over 10 days to apply controlled tension (Fig. 2G, left). For control wounds, distractors were affixed to wounds but not expanded; additionally, we applied and expanded distractors on uninjured skin. Mechanically loaded scars were grossly thickened and raised (Fig. 2G, far left versus center right photographs) and had the greatest YAP and α-SMA (activated/profibrotic myofibroblast marker) expression (Fig. 2H, bottom left), consistent with increased mechanotransduction. Tension also significantly increased pEPFs and YAP$^+$ cells in wounds (Fig. 2, H, bottom left, and I). It is conceivable that, through microscopic wound dehiscence, distraction caused increased inflammation, in turn driving *En1* activation. However, applying mechanical tension to unwounded skin also increased pEPFs and YAP$^+$ cells (Fig. 2,H, top right, and I). Although these findings do not exclude a role for other signals in regulating postnatal *En1* expression, they do suggest that mechanical forces are both necessary (no GFP$^+$ cells without tension) and sufficient for postnatal ENF-to-EPF transition.

After mechanical stimulation, YAP (mechanotransduction's final transcriptional effector) translocates to the nucleus, activating proliferation- and migration-related genes (Fig. 2F) (18, 19). YAP was shown to drive a feedback loop in lung fibroblasts sustaining pulmonary

fibrosis (19). We processed *En1*$^{Cre\text{-}ERT}$;*Ai6* YAP immunostaining through a colocalization analysis pipeline (Fig. 2J, top). Unwounded skin showed low nuclear YAP (Fig. 2J, middle left), consistent with minimal homeostatic mechanical activation. Wounds contained significantly more nuclear YAP$^+$ cells (Fig. 2J, middle center and right). Most high–nuclear YAP cells were ENFs (GFP$^-$CD26$^-$); eEPFs (GFP$^-$CD26$^+$) and pEPFs (GFP$^+$) showed comparatively lower nuclear YAP (Fig. 2J, bottom). To compare YAP signaling in ENFs and EPFs across the time course of healing, we next used our image analysis pipeline to compare YAP nuclear localization in excisional wound ENFs (CD26$^-$) and EPFs (CD26$^+$) at POD 0 (unwounded), 7, 14, and 30 (C57BL/6 mice). *En1*-negative fibroblasts rapidly activated YAP signaling by POD 7 and retained high nuclear YAP throughout the matrix deposition (POD 14) and early remodeling (POD 30) phases of wound healing (fig. S3). In contrast, most EPFs had no nuclear YAP at all time points, supporting a dominant role for YAP mechanotransduction signaling in ENFs.

We hypothesized that YAP promotes scarring predominantly by driving mechanoresponsive ENFs' transition to fibrotic pEPFs. We treated distracted incisional wounds with verteporfin (YAP inhibitor; Fig. 2F). Verteporfin mitigated the effects of tension: Verteporfin-treated mechanically loaded wounds grossly resembled non–mechanically loaded wounds (Fig. 2G, right) and contained significantly fewer pEPFs than nontreated mechanically loaded wounds (Fig. 2, H, bottom right, and I, top). Verteporfin treatment significantly decreased YAP and α-SMA expression (Fig. 2H, bottom right) and YAP$^+$ cells (Fig. 2I, bottom). Collectively, these results demonstrate that mechanical tension drives ENF-to-EPF transition in vivo in wounds.

Postnatally derived EPFs recapitulate embryonically derived EPF signatures

To elucidate the transcriptomic changes associated with postnatal *En1* activation, we subjected *En1*^{Cre};*R26*^{mTmG} ENFs grown on TCPS for 2, 7, or 14 days (when ENFs activate *En1*) (Fig. 3A) to bulk RNA sequencing (RNA-seq). Hierarchical clustering of genes whose expression was significantly up- or down-regulated after 14 days (factor of >4 change versus 2 days; fig. S4A) revealed a transcriptional shift (Fig. 3B and fig. S4B). Gene Ontology (GO) annotation (g.Profiler) revealed up-regulated ECM deposition–related terms (Fig. 3C, top), suggesting profibrotic changes, whereas muscle development–related terms were down-regulated (Fig. 3C, bottom). Gene set enrichment analysis (GSEA, Broad Institute) terms involving ECM production/deposition and epithelial-mesenchymal transition were up-regulated, and "muscle identity" terms down-regulated, after 14 days (fig. S4C). Native ENFs express muscle-related genes (10); these may be lost upon mechanical activation. Dlk1 expression was greatest at 7 days ("colony stage"; Fig. 3D, red box), consistent with disproportionate expansion of reticular ENFs driving increased Dlk1 expression at the bulk level. Consistent with g.Profiler and GSEA, multiple ECM genes (e.g., collagens, fibronectin) were up-regulated at 14 days (Fig. 3D, green box).

We next performed RNA-seq of papillary, reticular, and hypodermal ENFs after 2, 7, and 14 days on TCPS (fig. S5, A to C). All expressed low-level *En1* at 2 days, which suggests that

fibroblasts within all subpopulations are competent to express *En1.* By 14 days, papillary ENFs lacked evidence of mechanical activation but down-regulated translational machinery (GSEA; fig. S5, D and E, left); reticular and hypodermal ENFs up-regulated integrin-related terms, implying active mechanotransduction. Reticular ENFs activated *En1* and collagen-related GSEA terms (fig. S5, D and E, middle), but hypodermal ENFs did not up-regulate *En1*, instead showing activation of Wnt/TGF-β pathway and lipid- and collagen-related terms (fig. S5, D and E, right), potentially consistent with the previously reported "adipocyte precursor" fibroblast phenotype (20). Thus, although reticular and hypodermal ENFs were both mechanoresponsive on TCPS, only reticular ENFs activated *En1* and expressed a fibrogenic transcriptional program, consistent with in vivo findings (Fig. 1I).

Treating cells with verteporfin attenuated the transcriptomic shift in untreated cells (Fig. 3B, purple box). Upon principal components analysis (PCA), verteporfin-treated ENFs at 14 days more closely resembled untreated cells that had only been in culture for 2 days, consistent with diminished mechanical activation (fig. S4B, purple cluster). ECM-related GO terms were down-regulated, and muscle development-related terms up-regulated, in verteporfin-treated ENFs, suggesting closer retention of native ENF identity (Fig. 3C). ECM genes were also down-regulated with verteporfin (Fig. 3D, purple box), suggesting blocked profibrotic changes.

To study in vivo transcriptional changes, we subjected fibroblasts isolated from tamoxifen-induced $En1^{Cre\text{-}ERT};Ai6$ mice to RNA-seq: pEPFs (GFP^+) from wounds, and eEPFs (GFP^-CD26^+) and ENFs (GFP^-CD26^-) from skin and wounds (Fig. 3E). Upon hierarchical clustering (Fig. 3F) of differentially expressed genes after wounding (fig. S6A) and PCA (fig. S6B), pEPFs clustered more closely with eEPFs than with ENFs. pEPFs and eEPFs increased their expression of fibrosis-related genes, including *Dpp4* (CD26), upon wounding (fig. S2B and fig. S6C, left). ENFs up-regulated YAP signaling–related genes (Notch ligands *Jag1*, *Dll1*) (21), particularly after wounding, suggesting mechanoresponsiveness to the wound environment (fig. S6C, middle and right). By GSEA, scar ENFs were enriched for ECM adhesion– and Notch signaling– related terms, whereas pEPFs (putatively derived from mechanically activated ENFs) were enriched for ECM production– and ECM deposition–related terms (fig. S6D). Finally, we compared the transcriptional activity of genes previously reported to differentiate ENFs and eEPFs (Fig. 3G) (10). Again, pEPFs' gene expression profile most closely resembled that of eEPFs (Fig. 3G, green boxes). Thus, postnatal ENF *En1* activation, in vitro and in vivo, involved acquisition of a profibrotic, eEPF-like transcriptome.

Modulating YAP signaling promotes regenerative ENF-mediated wound healing

Because *En1* activation was associated with a profibrotic phenotype and blocked by YAP inhibition in vitro, we questioned whether YAP inhibition could block *En1* activation in vivo to reduce scarring. $En1^{Cre};R26^{mTmG}$ wounds were injected at POD 0 with phosphate-buffered saline (PBS; vehicle control) or verteporfin (1 mg/ml; no significant effect on healing rate, fig. S7A, red circles versus blue squares) and harvested at POD 14, 30, or 90.

Grossly, control wounds formed distinct, hairless scars (Fig. 4A, middle row); verteporfin-treated wounds had substantial hair growth by 30 days and were indistinguishable from unwounded skin by 90 days (Fig. 4A, bottom row). This result was notable, given that a hallmark of scars is the absence of secondary appendages [e.g., hair follicles (HF)/sebaceous glands (SG)]. Upon hematoxylin and eosin (H&E) staining, control wounds contained dense, parallel collagen without secondary elements (Fig. 4B, top). Verteporfin-treated wounds demonstrated reduced fibrosis with numerous HF/SG-like structures by 30 to 90 days (Fig. 4B, bottom, white arrowheads), which expressed cytokeratins 14 and 19 (CK14/19, HF/SG markers; Fig. 4C, top) and positive Oil Red O lipid staining (Fig. 4C, bottom), indicating functional regenerated HF and SG.

Whereas POD 14 control wounds contained abundant EPFs (GFP^+; Fig. 4D, top left), substantial col-I, and minimal fibronectin [Fn, reported as primary ENF-deposited matrix protein (22)] (Fig. 4D, top right; typical scar ECM), verteporfin-treated wounds contained predominantly ENFs ($tdTomato^+$; Fig. 4D, bottom left), substantially reduced col-I, and greater Fn (Fig. 4D, bottom right), suggesting blocked transition of ENFs into profibrotic pEPFs. POD 30 verteporfin-treated wounds had decreased EPFs and CD26 expression (versus controls; Fig. 4E, left). Whereas POD 30 control wounds had Dlk1 expression within deep dermis and chains of YAP^+ cells migrating into the scar (Fig. 4E, top), verteporfin-treated wounds had $Dlk1^+$ cells throughout the dermis and shorter YAP^+ chains (Fig. 4E, bottom). Collectively, these results suggest that mechanoresponsive$Dlk1^+Sca1^-$ ENFs proliferate and migrate after wounding, then activate *En1* to become fibrogenic pEPFs; blocking *En1* activation via mechanotransduction inhibition disrupts this process, resulting in $Dlk1^+$ ENFs throughout the wound. After 90 days, control scars had widespread EPFs and EPF-derived matrix (GFP^+), YAP^+ cells, and α-SMA expression consistent with profibrotic myofibroblasts (Fig. 4F, top). Verteporfin-treated wounds had fewer EPFs, rare YAP^+, and absent α-SMA^+ cells (Fig. 4F, bottom). $CD11b^+$ cell infiltrate (myeloid cells, important to scarring response) was comparable between PBS- and verteporfin-treated wounds throughout healing (fig. S8), which suggests that verteporfin's effects were not driven by altered immune response. Overall, these data support the idea that blocking ENF mechanical activation yields ENF-driven wound regeneration. In tamoxifen-induced $En1^{Cre\text{-}ERT};R26^{mTmG}$ mice, control wounds showed abundant GFP^+ cells after 14 days (Fig. 4G, top), whereas verteporfin-treated wounds showed few to none (Fig. 4G, bottom), confirming that verteporfin specifically inhibited ENF-to-pEPF transformation. These findings, together with observations that ENFs showed the highest YAP nuclear localization (Fig. 2J) and YAP-related gene expression (fig. S6C), suggest that verteporfin's wound-modulatory role specifically affects mechanoresponsive ENFs.

Visual analysis of gross histologic images is subjective and bias-prone (23, 24), so we sought to robustly confirmthat verteporfin prevented fibrosis by using a machine-learning algorithm to quantify tissue ultrastructure (25). Briefly, Picrosirius Red histology was color-deconvoluted to isolate ECM fiber components, which were noise-reduced and then binarized to digitally map thousands of fibers and branchpoints. Individual (e.g., length, width) and group (e.g., packing, alignment) fiber properties were calculated (see supplementary materials). Across multiple metrics, POD 14 verteporfin-treated wounds were quantitatively distinct from control wounds and were instead comparable to unwounded skin

(fig. S9, A and B). PCA of ECM parameters showed strong overlap between verteporfin and unwounded skin clusters at 14 days, increasing by 30 days, with complete overlap at 90 days (Fig. 4H and figs. S10 and S11), indicating that verteporfin treatment at POD 0 yielded long-term regenerative remodeling. Thus, quantitative analysis confirmed that YAP inhibition promotes wound regeneration.

We next assessed the effects of multiple verteporfin doses. Treatment with two doses (POD 0 and 4) yielded healing rates, gross appearance, ECM, and EPF abundances comparable to single-dose effects (POD 0) (fig. S7). When dosage was increased to four treatments (POD 0, 4, 8, and 12), EPFs were almost fully depleted (fig. S7, D and E) but wound closure was delayed, hair regrowth was reduced, and ECM features diverged from those of unwounded skin (fig. S7, A to C). Thus, verteporfin affected wounds in a dose-dependent manner, with detrimental effects upon excessive dosing.

Despite scars' excess collagen, they possess ≤80% of skin's strength because of inferior ECM organization (26). We sought to determine whether verteporfin-induced regeneration also functionally recovered skin's mechanical robustness. Consistent with scars' decreased structural integrity, POD 30 control wounds had significantly reduced tensile strength (versus skin; Fig. 4I, green versus red). In contrast, verteporfin-treated wounds' tensile strength did not significantly differ from that of unwounded skin (Fig. 4I, green versus blue), supporting restoration of unwounded-like strength (representative force-displacement/stress-strain curves, fig. S12).

Engrailed-1 is mechanically regulated and is required for skin scarring

The temporal relation between *En1* expression and profibrotic changes in vitro and in vivo suggested that *En1* itself may have a functional role in scarring (versus being a "bystander" marker). Using short hairpin RNA (shRNA), we achieved long-term *En1* knockdown in ENFs over 14 days on TCPS (fig. S13D). We compared RNA-seq to ENFs treated with nontargeting control shRNA (fig. S13, A to C). ECM production and deposition were significantly reduced with *En1* knockdown (decreased ECM-related GO enrichment; fig. S13E). GSEA showed down-regulation across mechanotransduction (*Rho/Notch/Hippo*) and fibrosis (*Jun/TGF*β) pathways (fig. S13F), which suggests that *En1* knockdown broadly decreases mechanically induced fibrogenic changes.

To assess whether *En1* expression is functionally related to fibrosis in vivo, we generated $En1^{Cre\text{-}ERT};Ai6;R26^{iDTR}$ mice and ablated pEPFs by administering diphtheria toxin (DT; control, PBS) upon wounding (Fig. 5A). Control wounds grossly yielded scars, but DT-treated wounds regenerated HF as early as 14 days, with thick tufts of hair by 30 days (Fig. 5B). Histology of DT-treated wounds revealed HF- and SG-like CK14/19^{+} structures (Fig. 5, C and D). Control wounds had abundant pEPFs (GFP^{+}; Fig. 5E, top), whereas DT-treated wounds exhibited near-complete pEPF ablation up to POD 30 (Fig. 5E, bottom right). Using our machine-learning approach (Fig. 4H), ECM architecture of control wounds (scars) diverged strongly from that of unwounded skin, with minimal or no overlap upon PCA (Fig. 5F); DT-treated wounds showed virtually complete overlap with unwounded skin (Fig. 5F), suggesting indistinguishable ultrastructure. These data suggest that ablating *En1*-activating

fibroblasts is sufficient for wound regeneration and, with our shRNA findings in vitro, may suggest that *En1* is itself a mechanoresponsive master regulator of fibroblast activation.

YAP knockout blocks *Engrailed-1* activation to promote ENF-mediated wound regeneration

To confirm that regeneration observed with verteporfin resulted from modulated mechanotransduction, rather than off-target effect(s) of the drug, we generated $En1^{Cre\text{-}ERT};R26^{mTmG};YAP^{fl/+}$ ($YAP^{fl/+}$) and $En1^{Cre\text{-}ERT};Ai6;YAP^{fl/fl}$ ($YAP^{fl/fl}$) mice for fibroblast-specific YAP deletion. We tamoxifen-induced and wounded $En1^{Cre\text{-}ERT};R26^{mTmG};YAP^{+/+}$ ($YAP^{+/+}$; control), $YAP^{fl/+}$, and $YAP^{fl/fl}$ mice and harvested wounds at POD 14 and 30. Grossly, $YAP^{+/+}$ wounds formed scars by 14 days (Fig. 6A, top). In contrast, $YAP^{fl/+}$ and $YAP^{fl/fl}$ wounds grew small hairs by 14 days, with substantial hair growth by 30 days (Fig. 6A, middle and bottom). Histologically, YAP knockout wounds regenerated HF/SG-like structures by 14 days and fully developed $CK14/19^{+}$ appendages by 30 days (Fig. 6, B, middle and bottom, and C, top and bottom). Unwounded skin in all models contained virtually no pEPFs, consistent with $En1^{Cre\text{-}ERT};Ai6$ mice (Fig. 6D, left; see also Fig. 1F). $YAP^{+/+}$ scars had numerous pEPFs at POD 14 and 30 (Fig. 6, D, top, and E, top), whereas only sparse pEPFs were observed in $YAP^{fl/+}$ and $YAP^{fl/fl}$ wounds (Fig. 6,D, middle and bottom, and E, top), confirming that YAP is required for postnatal *En1* activation. Immunofluorescent histology confirmed decreased YAP expression in $YAP^{fl/+}$ and $YAP^{fl/fl}$ mice (Fig. 6, D, far right, and E, bottom). Staining for EPF surrogate marker CD26 (Dpp4) revealed similar proportions of eEPFs ($GFP^{-}CD26^{+}$) in $YAP^{+/+}$ and $YAP^{fl/fl}$ wounds, which suggests that YAP knockout did not significantly affect existing eEPFs, but rather preferentially affected ENFs and their conversion to pEPFs (Fig. 6F).

Upon ECM ultrastructure quantitation, $YAP^{fl/+}$ wounds were quantitatively more similar to unwounded skin than were $YAP^{+/+}$ wounds (Fig. 6G, top); this effect was less pronounced than for verteporfin-treated and pEPF-ablated (Fig. 5) wounds, which suggests that heterozygous YAP deletion was insufficient for complete ultrastructural regeneration. $YAP^{fl/fl}$ homozygous knockout wounds were quantitatively indistinguishable from unwounded skin (Fig. 6G, bottom). This may reflect YAP signaling “dose-responsiveness” in mechanosensitive ENFs, with heterozygous loss of function conferring most but not all features of regeneration. Detrimental effects of excessive verteporfin dosing (fig. S7) were not observed in $YAP^{fl/fl}$ mice; we hypothesize that these reflect off-target effects of supratherapeutic verteporfin dosing, rather than direct effects of YAP inhibition. These findings support a functional role for YAP signaling in postnatal *En1* activation and scarring, because genetic YAP blockade in mechanoresponsive fibroblasts resulted in fewer pEPFs and regeneration.

Discussion

Fibroblasts are heterogeneous, comprising multiple subpopulations with distinct roles (10–12, 20, 22, 27–32). Wounding activates a dermal fibroblast subset to exhibit contractile properties and ECM production (33–36) that lead to fibrotic scar formation. We previously identified a dermal fibroblast subpopulation defined by embryonic *En1* expression (eEPFs)

responsible for dorsal scarring (10). However, the role of ENFs in postnatal wound healing was poorly understood. Here, we show that ENFs activate *En1* in response to wound mechanical cues and contribute to scarring as pEPFs.

Recent work categorized adult unwounded mouse skin fibroblasts into papillary, reticular, and hypodermal subdivisions (11, 12). Although based on anatomical location, these subpopulations may also confer differing fibrogenic potential. By anatomically fractionating ENFs, we identify $Dlk1^{+}Sca1^{-}$ reticular ENFs as the predominant mechanosensitive cell capable of postnatal *En1* activation. Other groups have reported subsets of α-$SMA^{+}CD26^{+}$ wound myofibroblasts arising from both *En1*- and *Dlk1*-traced fibroblast lineages (20, 37). Our findings support the importance of these lineages in wound healing and suggest that tissue mechanics may bridge these lineages (i.e., activate $Dlk1^{+}$ ENFs to $En1^{+}$ pEPFs), explaining their shared scarring role. A revised model of wound healing was also proposed recently, wherein superficial dermal injuries are repaired “classically” through EPF migration and local matrix deposition, whereas deep dermal injuries are plugged or otherwise repaired by provisional “primordium” steered upward by fascial fibroblasts (38). However, we note that (i) no wounds in this study involved fascia; (ii) in vivo pEPFs were not noted outside the dermis; and (iii) reticular dermal fibroblasts were the dominant pEPF source in all experiments. Given that the vast majority of scarring injuries in humans do not involve fascia, the mechanosensitive, reticular dermal fibroblast population identified by our study, and mechanisms guiding its contribution to fibrosis, may be of greater clinical relevance for scarring.

Despite preserving much of the molecular machinery displayed by regenerating organisms, mammals have limited regenerative potential because of their propensity for rapid scarring. Human scarring is augmented by high skin tension, a 100,000-year-old selective adaption that virtually precludes regenerative wound healing (1). Tension’s contribution to scarring is well recognized by surgeons, who classically incise along relaxed skin tension lines to minimize scarring. Previous work from our group and others has shown that physical tension offloading significantly reduces scarring, as does chemically blocking cellular mechanotransduction (FAK inhibition) (16, 17, 39). However, specific cell populations involved in the profibrotic tension response and their mechanisms of mechanical activation were unknown. By precisely delineating how physical stimuli provoke $Dlk1^{+}$ ENFs toward fibrosis, we identify YAP and *En1* as promising molecular targets to prevent scarring. Furthermore, we show that YAP inhibition prevents *En1* activation in wounds, encouraging ENF-mediated, regenerative, nonfibrotic repair. This work demonstrates fully regenerative skin healing in a typically scarring postnatal mammal. We hypothesize that YAP inhibition, through targeted modulation of profibrotic pathways in specific fibroblasts, enables regeneration without compromising healing. Preventing the fibrotic response permits regeneration over months or longer, which suggests that mammalian regeneration may be unlocked if mechanically driven fibrosis can be blocked. Early evidence suggests that ENF-mediated healing after verteporfin treatment leads to recovery of normal skin glands, hair follicles, and matrix ultrastructure through activation of Wnt/Trps1 stem cell and hair follicle development pathways (25).

Scar-reducing strategies often entail ablating fibrogenic cell populations, which can potentially impair healing by nonspecifically eliminating necessary cells (5, 7, 8). Thus, the therapeutic goal of skin regeneration—defined by recovery of secondary elements, ECM structure, and mechanical strength—has remained unachieved. The finding that ENF-mediated postnatal healing satisfies these criteria for regeneration without compromising healing speed or efficacy implies that regeneration may represent a “default” wound repair pathway, superseded by the emergence of scarring EPFs. Our data support the notion that it is not the amount of collagen and ECM that determines a scar, but rather the relative organization of the total ECM. For example, pathological scars in humans (hypertrophic scars, keloids) contain elevated collagen levels but have weaker material properties than unwounded skin because they lack its basket-weave ECM organization. In contrast, verteporfin-treated wounds are as strong as unwounded skin because their ECM organization is identical. Tipping the balance of healing toward ENFs via YAP inhibition alters both ECM protein content and reorganization, and so this should not be viewed as only decreasing collagen deposition. Recently, it was reported that activation of YAP mechanosignaling promotes liver fibrosis and that promoting YAP degradation blocks the progression of liver cirrhosis (40); thus, it is possible that our findings regarding YAP signaling in skin scarring are relevant to fibrotic responses in other organs and could have similar therapeutic implications.

Methods summary

Fibroblast subpopulations (e.g., *En1*-positive and -negative) were isolated from mouse dorsal skin via enzymatic digestion and flow cytometry (FACS). FACS-purified fibroblasts were engrafted into dorsal skin of wild-type mice; the engrafted region was then wounded to observe the response of fibroblast subtypes to the wound environment. For in vitro experiments, FACS-purified fibroblasts were cultured either on stiff tissue culture plastic or in soft collagen hydrogels. For transcriptomic profiling, fibroblasts were subjected to bulk RNA-seq. For excisional wounding, circular, full-thickness sections of dorsal skin (extending to the panniculus carnosus) were cut out and the skin was splinted with silicone rings to prevent contraction. For incisional wounding, longitudinal, full-thickness incisions were made in the dorsal skin and a loading device was secured to apply tension perpendicular to the line of incision. Wounds were injected with PBS (vehicle control) or verteporfin resuspended in PBS and were then analyzed over the course of healing by gross visual examination, histologic analyses, and mechanical strength testing. Transgenic mouse strains were used to fluorescently trace fibroblast lineages and/or selectively ablate fibroblast subpopulations (e.g., YAP- or *En1*-expressing). For quantitative comparison of extracellular matrices, an image-processing algorithm was used to profile 26 ultrastructural features from Picrosirius Red–stained histology. For more detailed methods, see supplementary materials.

Supplementary Material

Refer to Web version on PubMed Central for supplementary material.

ACKNOWLEDGMENTS

We thank the Stanford Functional Genomics Facility, Stanford Cell Sciences Imaging Facility, Stanford Nano Shared Facilities, and Stanford Shared FACS Facility Cores. We also thank M. Januszyk for review of the manuscript and helpful suggestions.

Funding:

Supported by the Hagey Laboratory for Pediatric Regenerative Medicine (M.T.L., D.C.W., G.C.G., and H.P.L.); the Gunn/Olivier Research Fund, the Stinehart/Reed Award, and NIH grant R01-GM136659 (M.T.L.); and NIH grants R01-GM116892 (H.P.L. and M.T.L.), R01-DE027346 (D.C.W. and M.T.L.), and U24-DE026914 (D.C.W., G.C.G., and M.T.L.).

Data and materials availability:

All data to support the conclusions in this manuscript can be found in the figures and the supplementary materials. Any other data can be requested from the corresponding authors. RNA-seq data and Matlab code can be accessed from the following Github repository: https://github.com/shamikmascharak/Mascharak-et-al-ENF. M.T.L., S.M., H.E.dJ.-P., M.R.B., and M.F.D. are inventors on patent 62/879,369 held by Stanford University that covers use of YAP inhibition for wound healing. S.M., H.E.dJ.-P., M.R.B., A.L.M., and M.T.L. are inventors on patent application PCT/US2020/043717 that covers a machine-learning algorithm for analysis of connective tissue networks in scarring and chronic fibroses.

Appendix

Appendix

INTRODUCTION:

Skin wounds generally heal by scarring, a fibrotic process mediated by the *Engrailed-1* (*En1*) fibroblast lineage. Scars differ from normal unwounded skin in three ways: (i) They lack hair follicles, sebaceous glands, and other dermal appendages; (ii) they contain dense, parallel extracellular matrix fibers rather than the “basket-weave” pattern of uninjured skin; and (iii) as a result of this altered matrix structure, they lack skin’s normal flexibility and strength. A successful scar therapy would address these three differences by promoting regrowth of dermal appendages, reestablishment of normal matrix ultrastructure, and restoration of mechanical robustness. However, little is known about the cellular and molecular mechanisms blocking a regenerative healing response in postnatal skin, or whether these mechanisms can be bypassed by modulating specific fibroblast lineages.

RATIONALE:

We asked whether scarring fibroblasts are derived purely from expansion of existing *En1* lineage–positive fibroblasts present in unwounded skin, or whether *En1* scar fibroblasts could arise de novo by activation of *En1* expression in postnatal, *En1* lineage–negative fibroblasts within the wound niche. We used fibroblast transplantation as well as transgenic mouse models to trace *En1* expression in a spatiotemporally defined fashion. Next, we studied fibroblast responses to mechanical forces in vitro and in vivo to establish a

mechanotransduction mechanism linking skin tension to postnatal *En1* expression. Finally, we used chemical (verteporfin) and transgenic inhibition of mechanotransduction signaling [diphtheria toxin ablation of *En1*-expressing fibroblasts, floxed Yes-associated protein (YAP) knockout] to modulate *En1* expression during wound healing. Experimental wounds were compared to unwounded skin and scars (phosphate-buffered saline control) by RNA sequencing, quantitative histopathological comparison (using a custom image-processing algorithm), and mechanical strength testing.

RESULTS:

Fibroblast transplantation and lineage-tracing studies reveal that *En1* lineage–negative fibroblasts (ENFs) of the reticular (deep) dermis activate *En1* in the wound environment, generating ~40 to 50% of scar fibroblasts. This phenomenon depends on mechanical cues: ENFs cultured on soft substrates or treated with chemical inhibitors of mechanical signaling proteins (e.g., YAP) do not activate *En1*. Comparison of ENFs with *En1*-expressing and *En1* knockdown (short hairpin RNA) fibroblasts by RNA sequencing suggests that *En1* regulates a wide array of genes related to skin fibrosis. In healing wounds, YAP inhibition by verteporfin blocks *En1* activation and promotes ENF-mediated repair, yielding skin regeneration in 30 days with recovery of functional hair follicles and sebaceous glands. Quantitative comparison of scars and regenerated skin shows that YAP inhibition induces recovery of normal dermal ultrastructure, which in turn confers restoration of normal mechanical breaking strength. Diphtheria toxin–mediated ablation of postnatal *En1*-expressing fibroblasts and fibroblast-targeted transgenic YAP knockout similarly promoted recovery of normal skin structures, which suggests that modulation of *En1* activation, whether direct or indirect, can yield wound regeneration.

CONCLUSION:

By delineating how physical stimuli provoke ENFs to contribute to fibrosis, we identify YAP and *En1* as possible molecular targets to prevent scarring. Furthermore, we have shown that inhibition of YAP signaling prevents *En1* activation during wound healing, thus encouraging ENF-mediated wound repair without fibrosis and with regeneration of secondary skin elements (hair follicles, sebaceous glands). Our findings suggest that residual ENFs in postnatal mammalian skin retain a capacity for skin regeneration if the mechanically driven propensity for fibrosis can be blocked. We have demonstrated fully regenerative skin healing in a postnatal mammal that normally scars; this finding has translational implications for the tens of millions of patients each year who develop scars and other fibroses.

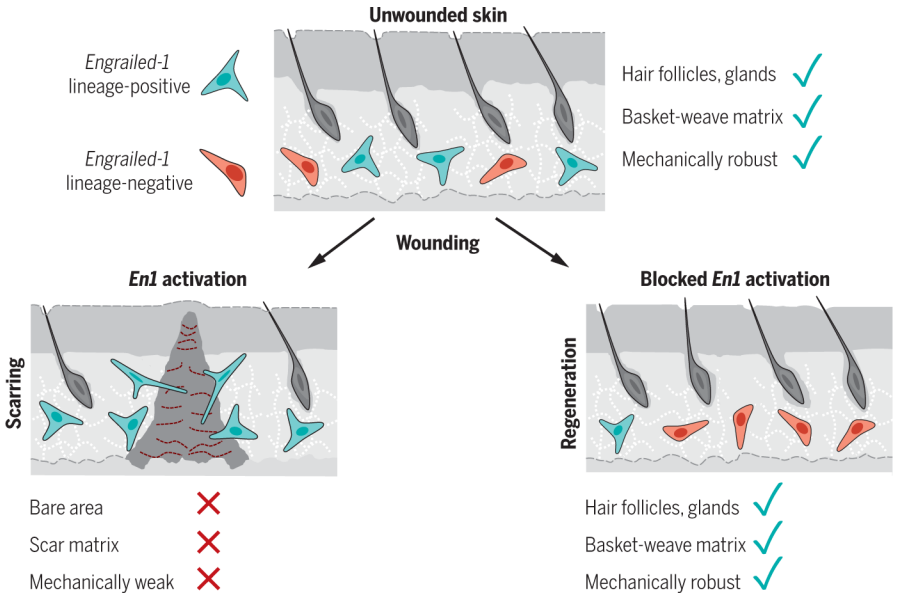

***Engrailed-1* activation in skin fibroblasts drives scarring.**

After injury, a subset of dermal fibroblasts activates *Engrailed-1* (*En1*) to contribute to scarring (left). Inhibiting postnatal *En1* activation, either directly (by ablating *En1*-activating cells) or indirectly (by blocking mechanical signaling with verteporfin), promotes skin regeneration by *En1* lineage-negative fibroblasts, with full recovery of normal hair follicles, glands, matrix ultrastructure, and mechanical strength. Green cells, *En1* lineage-positive fibroblasts; red cells, *En1* lineage-negative fibroblasts.

References

1. Gurtner GC, Werner S, Barrandon Y, Longaker MT, Wound repair and regeneration. Nature 453, 314–321 (2008). doi:10.1038/nature07039 [PubMed: 18480812]
2. Bayat A, McGrouther DA, Ferguson MW, Skin scarring. BMJ 326, 88–92 (2003). doi:10.1136/bmj.326.7380.88 [PubMed: 12521975]
3. Eming SA, Martin P, Tomic-Canic M, Wound repair and regeneration: Mechanisms, signaling, and translation. Sci. Transl. Med. 6, 265sr6 (2014). doi:10.1126/scitranslmed.3009337 [PubMed: 25473038]
4. Sun BK, Siprashvili Z, Khavari PA, Advances in skin grafting and treatment of cutaneous wounds. Science 346, 941–945 (2014). doi:10.1126/science.1253836 [PubMed: 25414301]
5. Griffin MF, desJardins-Park HE, Mascharak S, Borrelli MR, Longaker MT, Understanding the impact of fibroblast heterogeneity on skin fibrosis. Dis. Model. Mech 13, dmm044164 (2020). doi:10.1242/dmm.044164 [PubMed: 32541065]
6. Sen CK, Gordillo GM, Roy S, Kirsner R, Lambert L, Hunt TK, Gottrup F, Gurtner GC, Longaker MT, Human skin wounds: A major and snowballing threat to public health and the economy. Wound Repair Regen. 17, 763–771 (2009). doi:10.1111/j.1524-475X.2009.00543.x [PubMed: 19903300]
7. desJardins-Park HE, Chinta MS, Foster DS, Borrelli MR, Shen AH, Wan DC, Longaker MT, Fibroblast Heterogeneity in and Its Implications for Plastic and Reconstructive Surgery. Plast. Reconstr. Surg. Glob. Open 8, e2927 (2020). doi:10.1097/GOX.0000000000002927 [PubMed: 32766071]
8. Mascharak S, desJardins-Park HE, Longaker MT, Fibroblast Heterogeneity in Wound Healing: Hurdles to Clinical Translation. Trends Mol. Med. 26, 1101–1106 (2020). doi:10.1016/j.molmed.2020.07.008 [PubMed: 32800679]

9. Walmsley GG, Maan ZN, Wong VW, Duscher D, Hu MS, Zielins ER, Wearda T, Muhonen E, McArdle A, Tevlin R, Atashroo DA, Senarath-Yapa K, Lorenz HP, Gurtner GC, Longaker MT, Scarless wound healing: Chasing the holy grail. Plast. Reconstr. Surg. 135, 907–917 (2015). doi:10.1097/PRS.0000000000000972 [PubMed: 25719706]
10. Rinkevich Y, Walmsley GG, Hu MS, Maan ZN, Newman AM, Drukker M, Januszyk M, Krampitz GW, Gurtner GC, Lorenz HP, Weissman IL, Longaker MT, Identification and isolation of a dermal lineage with intrinsic fibrogenic potential. Science 348, aaa2151 (2015). doi:10.1126/science.aaa2151 [PubMed: 25883361]
11. Driskell RR, Lichtenberger BM, Hoste E, Kretzschmar K, Simons BD, Charalambous M, Ferron SR, Herault Y, Pavlovic G, Ferguson-Smith AC, Watt FM, Distinct fibroblast lineages determine dermal architecture in skin development and repair. Nature 504, 277–281 (2013). doi:10.1038/nature12783 [PubMed: 24336287]
12. Driskell RR, Watt FM, Understanding fibroblast heterogeneity in the skin. Trends Cell Biol. 25, 92–99 (2015). doi:10.1016/j.tcb.2014.10.001 [PubMed: 25455110]
13. Provenzano PP, Keely PJ, Mechanical signaling through the cytoskeleton regulates cell proliferation by coordinated focal adhesion and Rho GTPase signaling. J. Cell Sci. 124, 1195–1205 (2011). doi:10.1242/jcs.067009 [PubMed: 21444750]
14. Barnes LA, Marshall CD, Leavitt T, Hu MS, Moore AL, Gonzalez JG, Longaker MT, Gurtner GC, Mechanical Forces in Cutaneous Wound Healing: Emerging Therapies to Minimize Scar Formation. Adv. Wound Care 7, 47–56 (2018). doi:10.1089/wound.2016.0709
15. Aarabi S, Bhatt KA, Shi Y, Paterno J, Chang EI, Loh SA, Holmes JW, Longaker MT, Yee H, Gurtner GC, Mechanical load initiates hypertrophic scar formation through decreased cellular apoptosis. FASEB J. 21, 3250–3261 (2007). doi:10.1096/fj.07-8218com [PubMed: 17504973]
16. Wong VW, Rustad KC, Akaishi S, Sorkin M, Glotzbach JP, Januszyk M, Nelson ER, Levi K, Paterno J, Vial IN, Kuang AA, Longaker MT, Gurtner GC, Focal adhesion kinase links mechanical force to skin fibrosis via inflammatory signaling. Nat. Med. 18, 148–152 (2011). doi:10.1038/nm.2574 [PubMed: 22157678]
17. Longaker MT, Rohrich RJ, Greenberg L, Furnas H, Wald R, Bansal V, Seify H, Tran A, Weston J, Korman JM, Chan R, Kaufman D, Dev VR, Mele JA, Januszyk M, Cowley C, McLaughlin P, Beasley B, Gurtner GC, A randomized controlled trial of the embrace advanced scar therapy device to reduce incisional scar formation. Plast. Reconstr. Surg. 134, 536–546 (2014). doi:10.1097/PRS.0000000000000417 [PubMed: 24804638]
18. Panciera T, Azzolin L, Cordenonsi M, Piccolo S, Mechanobiology of YAP and TAZ in physiology and disease. Nat. Rev. Mol. Cell Biol. 18, 758–770 (2017). doi:10.1038/nrm.2017.87 [PubMed: 28951564]
19. Liu F, Lagares D, Choi KM, Stopfer L, Marinković A, Vrbanac V, Probst CK, Hiemer SE, Sisson TH, Horowitz JC, Rosas IO, Fredenburgh LE, Feghali-Bostwick C, Varelas X, Tager AM, Tschumperlin DJ, Mechanosignaling through YAP and TAZ drives fibroblast activation and fibrosis. Am. J. Physiol. Lung Cell. Mol. Physiol. 308, L344–L357 (2015). doi:10.1152/ajplung.00300.2014 [PubMed: 25502501]
20. Shook BA, Wasko RR, Rivera-Gonzalez GC, Salazar-Gatzimas E, López-Giráldez F, Dash BC, Muñoz-Rojas AR, Aultman KD, Zwick RK, Lei V, Arbiser JL, Miller-Jensen K, Clark DA, Hsia HC, Horsley V, Myofibroblast proliferation and heterogeneity are supported by macrophages during skin repair. Science 362, eaar2971 (2018). doi:10.1126/science.aar2971 [PubMed: 30467144]
21. Totaro A, Castellan M, Di Biagio D, Piccolo S, Crosstalk between YAP/TAZ and Notch Signaling. Trends Cell Biol. 28, 560–573 (2018). doi:10.1016/j.tcb.2018.03.001 [PubMed: 29665979]
22. Jiang D, Correa-Gallegos D, Christ S, Stefanska A, Liu J, Ramesh P, Rajendran V, De Santis MM, Wagner DE, Rinkevich Y, Two succeeding fibroblastic lineages drive dermal development and the transition from regeneration to scarring. Nat. Cell Biol. 20, 422–431 (2018). doi:10.1038/s41556-018-0073-8 [PubMed: 29593327]
23. Eva KW, Norman GR, Heuristics and biases—A biased perspective on clinical reasoning. Med. Educ 39, 870–872 (2005). doi:10.1111/j.1365-2929.2005.02258.x [PubMed: 16150023]
24. Tversky A, Kahneman D, Judgment under Uncertainty: Heuristics and Biases. Science 185, 1124–1131 (1974). doi:10.1126/science.185.4157.1124 [PubMed: 17835457]

25. Mascharak S et al. , Diverging molecular signatures of regeneration and fibrosis during wound repair. bioRxiv 2020.12.17.423181 [preprint]. 18 December 2020.
26. Marshall CD, Hu MS, Leavitt T, Barnes LA, Lorenz HP, Longaker MT, Cutaneous Scarring: Basic Science, Current Treatments, and Future Directions. Adv. Wound Care 7, 29–45 (2018). doi:10.1089/wound.2016.0696
27. Marsh E, Gonzalez DG, Lathrop EA, Boucher J, Greco V, Positional Stability and Membrane Occupancy Define Skin Fibroblast Homeostasis In Vivo. Cell 175, 1620–1633.e13 (2018). doi:10.1016/j.cell.2018.10.013 [PubMed: 30415836]
28. Salzer MC, Lafzi A, Berenguer-Llergo A, Youssif C, Castellanos A, Solanas G, Peixoto FO, Stephan-Otto Attolini C, Prats N, Aguilera M, Martín-Caballero J, Heyn H, Benitah SA, Identity Noise and Adipogenic Traits Characterize Dermal Fibroblast Aging. Cell 175, 1575–1590.e22 (2018). doi:10.1016/j.cell.2018.10.012 [PubMed: 30415840]
29. Tabib T, Morse C, Wang T, Chen W, Lafyatis R, SFRP2/DPP4 and FMO1/LSP1 Define Major Fibroblast Populations in Human Skin. J. Invest. Dermatol. 138, 802–810 (2018). doi:10.1016/j.jid.2017.09.045 [PubMed: 29080679]
30. Lynch MD, Watt FM, Fibroblast heterogeneity: Implications for human disease. J. Clin. Invest. 128, 26–35 (2018). doi:10.1172/JCI93555 [PubMed: 29293096]
31. Philippeos C, Telerman SB, Oulès B, Pisco AO, Shaw TJ, Elgueta R, Lombardi G, Driskell RR, Soldin M, Lynch MD, Watt FM, Spatial and Single-Cell Transcriptional Profiling Identifies Functionally Distinct Human Dermal Fibroblast Subpopulations. J. Invest. Dermatol. 138, 811–825 (2018). doi:10.1016/j.jid.2018.01.016 [PubMed: 29391249]
32. Leavitt T, Hu MS, Borrelli MR, Januszyk M, Garcia JT, Ransom RC, Mascharak S, desJardins-Park HE, Litzenburger UM, Walmsley GG, Marshall CD, Moore AL, Duoto B, Adem S, Foster DS, Salhotra A, Shen AH, Griffin M, Shen EZ, Barnes LA, Zielins ER, Maan ZN, Wei Y, Chan CKF, Wan DC, Lorenz HP, Chang HY, Gurtner GC, Longaker MT, Prrx1 Fibroblasts Represent a Pro-fibrotic Lineage in the Mouse Ventral Dermis. Cell Rep. 33, 108356 (2020). doi:10.1016/j.celrep.2020.108356 [PubMed: 33176144]
33. Darby IA, Hewitson TD, Fibroblast differentiation in wound healing and fibrosis. Int. Rev. Cytol. 257, 143–179 (2007). doi:10.1016/S0074-7696(07)57004-X [PubMed: 17280897]
34. Darby IA, Laverdet B, Bonté F, Desmoulière A, Fibroblasts and myofibroblasts in wound healing. Clin. Cosmet. Investig. Dermatol. 7, 301–311 (2014).
35. Hinz B, Formation and function of the myofibroblast during tissue repair. J. Invest. Dermatol. 127, 526–537 (2007). doi:10.1038/sj.jid.5700613 [PubMed: 17299435]
36. Hinz B, Phan SH, Thannickal VJ, Galli A, Bochaton-Piallat M-L, Gabbiani G, The myofibroblast: One function, multiple origins. Am. J. Pathol. 170, 1807–1816 (2007). doi:10.2353/ajpath.2007.070112 [PubMed: 17525249]
37. Guerrero-Juarez CF, Dedhia PH, Jin S, Ruiz-Vega R, Ma D, Liu Y, Yamaga K, Shestova O, Gay DL, Yang Z, Kessenbrock K, Nie Q, Pear WS, Cotsarelis G, Plikus MV, Single-cell analysis reveals fibroblast heterogeneity and myeloid-derived adipocyte progenitors in murine skin wounds. Nat. Commun. 10, 650 (2019). doi:10.1038/s41467-018-08247-x [PubMed: 30737373]
38. Correa-Gallegos D, Jiang D, Christ S, Ramesh P, Ye H, Wannemacher J, Kalgudde Gopal S, Yu Q, Aichler M, Walch A, Mirastschijski U, Volz T, Rinkevich Y, Patch repair of deep wounds by mobilized fascia. Nature 576, 287–292 (2019). doi:10.1038/s41586-019-1794-y [PubMed: 31776510]
39. Lim AF, Weintraub J, Kaplan EN, Januszyk M, Cowley C, McLaughlin P, Beasley B, Gurtner GC, Longaker MT, The embrace device significantly decreases scarring following scar revision surgery in a randomized controlled trial. Plast. Reconstr. Surg. 133, 398–405 (2014). doi:10.1097/01.prs.0000436526.64046.d0 [PubMed: 24105084]
40. Alsamman S, Christenson SA, Yu A, Ayad NME, Mooring MS, Segal JM, Hu JK-H, Schaub JR, Ho SS, Rao V, Marlow MM, Turner SM, Sedki M, Pantano L, Ghoshal S, Ferreira DDS, Ma H-Y, Duwaerts CC, Espanol-Suner R, Wei L, Newcomb B, Mileva I, Canals D, Hannun YA, Chung RT, Mattis AN, Fuchs BC, Tager AM, Yimlamai D, Weaver VM, Mullen AC, Sheppard D, Chen JY, Targeting acid ceramidase inhibits YAP/TAZ signaling to reduce fibrosis in mice. Sci. Transl. Med. 12, eaay8798 (2020). doi:10.1126/scitranslmed.aay8798 [PubMed: 32817366]

41. Stauffer W, Sheng H, Lim HN, EzColocalization: An ImageJ plugin for visualizing and measuring colocalization in cells and organisms. Sci. Rep. 8, 15764 (2018). doi:10.1038/s41598-018-33592-8 [PubMed: 30361629]

42. Ruifrok AC, Johnston DA, Quantification of histochemical staining by color deconvolution. Anal. Quant. Cytol. Histol. 23, 291–299 (2001). [PubMed: 11531144]

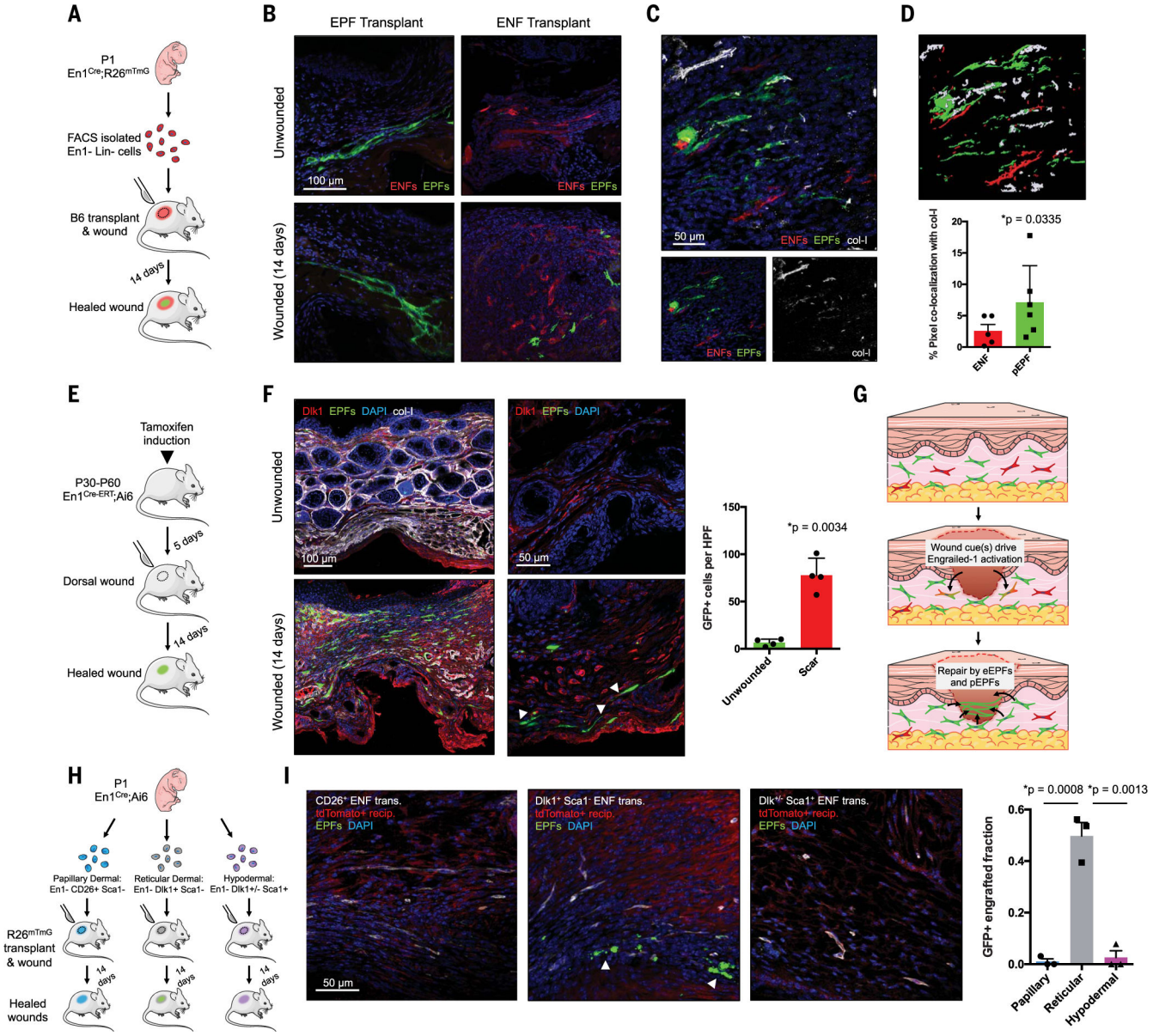

Fig. 1. Deep dermal ENFs activate *Engrailed-1* and contribute to postnatal scar collagen deposition.

(**A**) Schematic depicting cell transplantation, engraftment, and wounding experiments. (**B**) Confocal imaging of transplanted *En1*-positive fibroblasts (EPFs) and *En1*-negative fibroblasts (ENFs) before and after wounding [includes 4′,6-diamidino-2-phenylindole (DAPI, blue)]. (**C**) ENF transplantation and wounding, with postnatal EPFs (pEPFs, green) derived from ENF-to-EPF conversion; immunostaining for type I collagen (col-I). (**D**) Top: 3D reconstruction of (C). Bottom: Colocalization between col-I and tdTomato (ENF) or GFP (pEPF) signal. (**E**) Schematic depicting induction and wounding of *En1*$^{Cre\text{-}ERT}$*;Ai6* mice for temporally defined assessment of *En1* activation. (**F**) Left: Skin and wounds of tamoxifen-induced *En1*$^{Cre\text{-}ERT}$*;Ai6* mice; EPFs (white arrowheads) necessarily arose from *En1* expression during healing. Immunostaining for Dlk1, col-I. Right: Quantification of

GFP$^+$ cells (pEPFs) in unwounded skin or scars; paired two-tailed *t* test. (**G**) Proposed mechanism for postnatal *En1* activation. Dermal ENFs (red) exposed to wound-specific cues convert to pEPFs, which, with embryonically derived EPFs (eEPFs), mediate scarring. (**H**) Schematic depicting ENF subtype isolation, transplantation, and wounding. (**I**) Left: Papillary (CD26$^+$, left), reticular (Dlk1$^+$Sca1$^-$, center), and hypodermal (Dlk1$^{+/-}$Sca1$^+$, right) ENFs in wounded tdTomato$^+$ recipient (red); only reticular ENFs become pEPFs (white arrowheads). Right: Quantification of pEPFs in subtype-engrafted wounds.

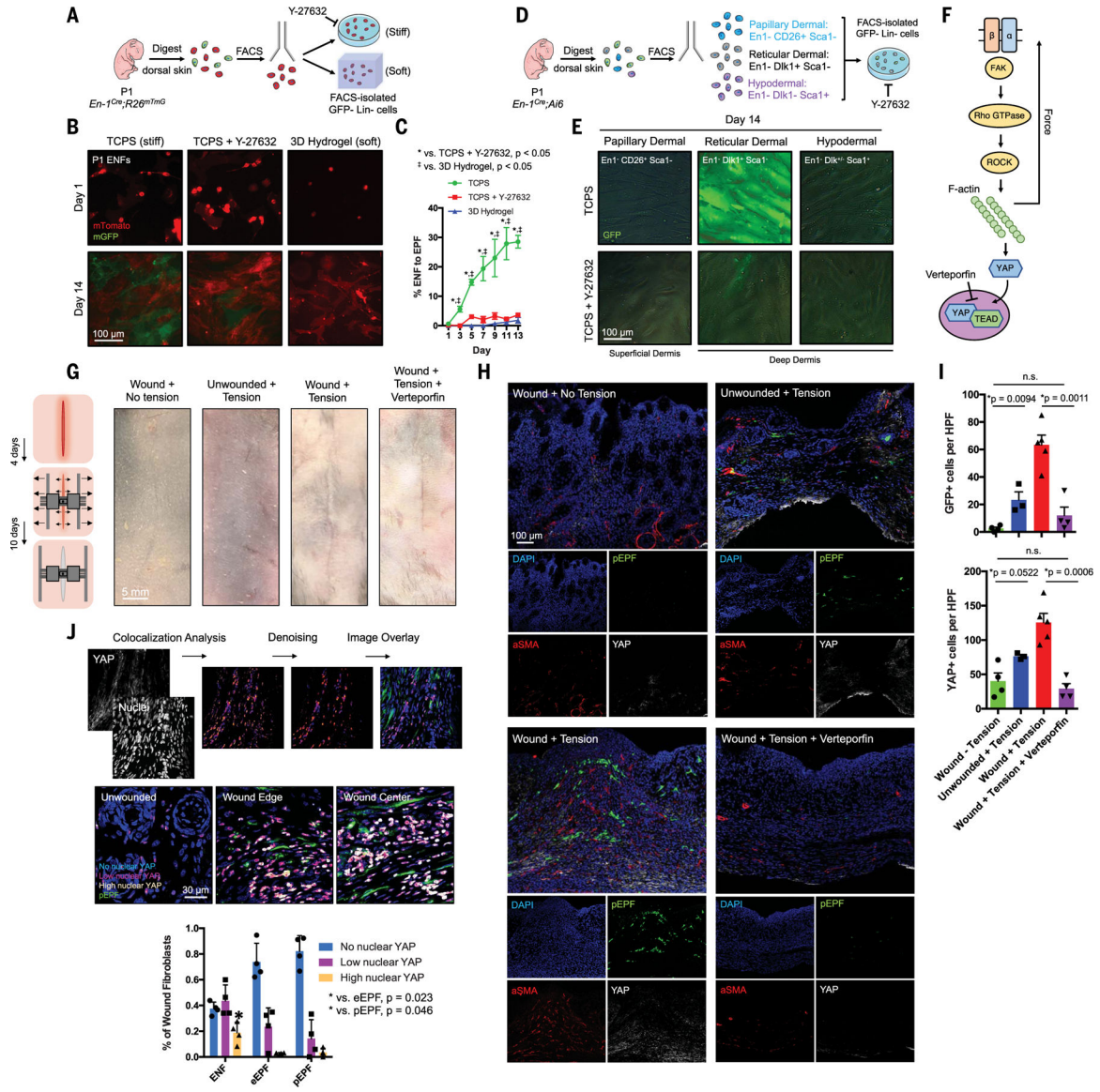

Fig. 2. Reticular dermal ENFs activate *Engrailed-1* via canonical mechanotransduction signaling in response to in vitro and in vivo substrate mechanics.

(**A**) Schematic depicting ENF culture on mechanically varied substrates. (**B**) ENFs (red) cultured on stiff TCPS with or without ROCK inhibitor (Y-27632) or soft hydrogel variably convert to pEPFs (green). (**C**) Quantification of ENF-to-EPF conversion by condition. (**D**) Schematic depicting ENF subpopulation culture on TCPS with or without Y-27632. (**E**) Cultured ENF subtypes show *En1* activation (green) only in reticular dermal ENFs on TCPS. (**F**) Schematic of canonical mechanotransduction signaling. Verteporfin inhibits YAP, the pathway's transcriptional effector. (**G**) Left: Schematic depicting wound tension/distraction. Right: Photographs of skin and wounds with or without tension and verteporfin treatment. (**H**) Fluorescent histology of the four conditions in (G) in *En1*$^{Cre\text{-}ERT}$*;Ai6* showing increased pEPFs (green) with increased tension. Immunofluorescent staining for α-SMA and YAP. (**I**) Quantification of pEPFs (top) and YAP^{+} cells (bottom) per 20× high-power field (HPF); n.s., not significant. (**J**) Top: Pipeline to quantify nuclear YAP. Middle: Overlaid images

showing nuclear YAP localization in skin/wound regions. Bottom: Quantification of nuclear YAP levels in ENFs, eEPFs, and pEPFs showing significantly more high–nuclear YAP ENFs than eEPFs or pEPFs.

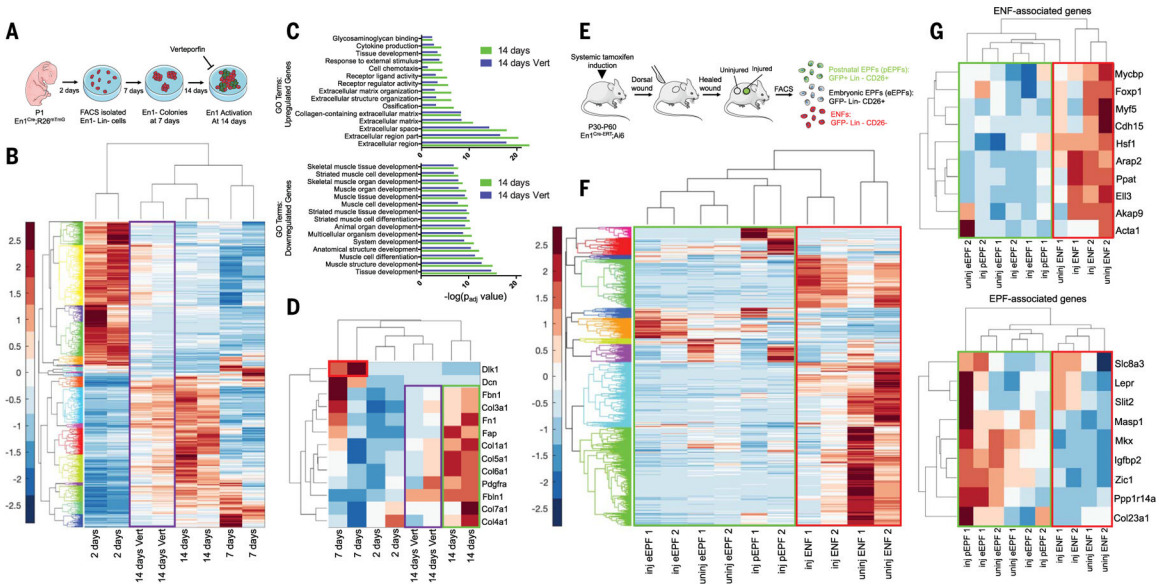

Fig. 3. Mechanical activation of Dlk1^{+} ENFs is associated with a fibrotic transcriptional signature.

(**A**) Schematic of bulk ENF culture over time, with or without verteporfin. (**B**) Gene expression heatmap and hierarchical clustering for 920 genes significantly up- or down-regulated (by a factor of >4) at 14 days in culture (versus 2 days). Values are shown for 2, 7, or 14 days in culture and 14 days with verteporfin (Vert; purple box). (**C**) GO term enrichments for significantly up-regulated (top) and down-regulated (bottom) genes from (B), at 14 days with or without Vert. (**D**) Heatmap showing relative expression of selected genes previously implicated in fibrosis/ECM deposition. Dlk1 expression was up-regulated in ENFs at 7 days (red box). Profibrotic/matrix genes were up-regulated at 14 days (green box) but mitigated by Vert (purple box). (**E**) Schematic depicting isolation of skin and scar pEPFs, eEPFs, and ENFs for RNA-seq. (**F**) Heatmap and hierarchical clustering of 1138 genes significantly up- or down-regulated in ENFs, eEPFs, or pEPFs in wounds (inj) versus skin (uninj). (**G**) Heatmaps showing relative expression of selected genes previously associated with ENF (top) or EPF (bottom) identity. Green boxes, EPF populations; red boxes, ENFs.

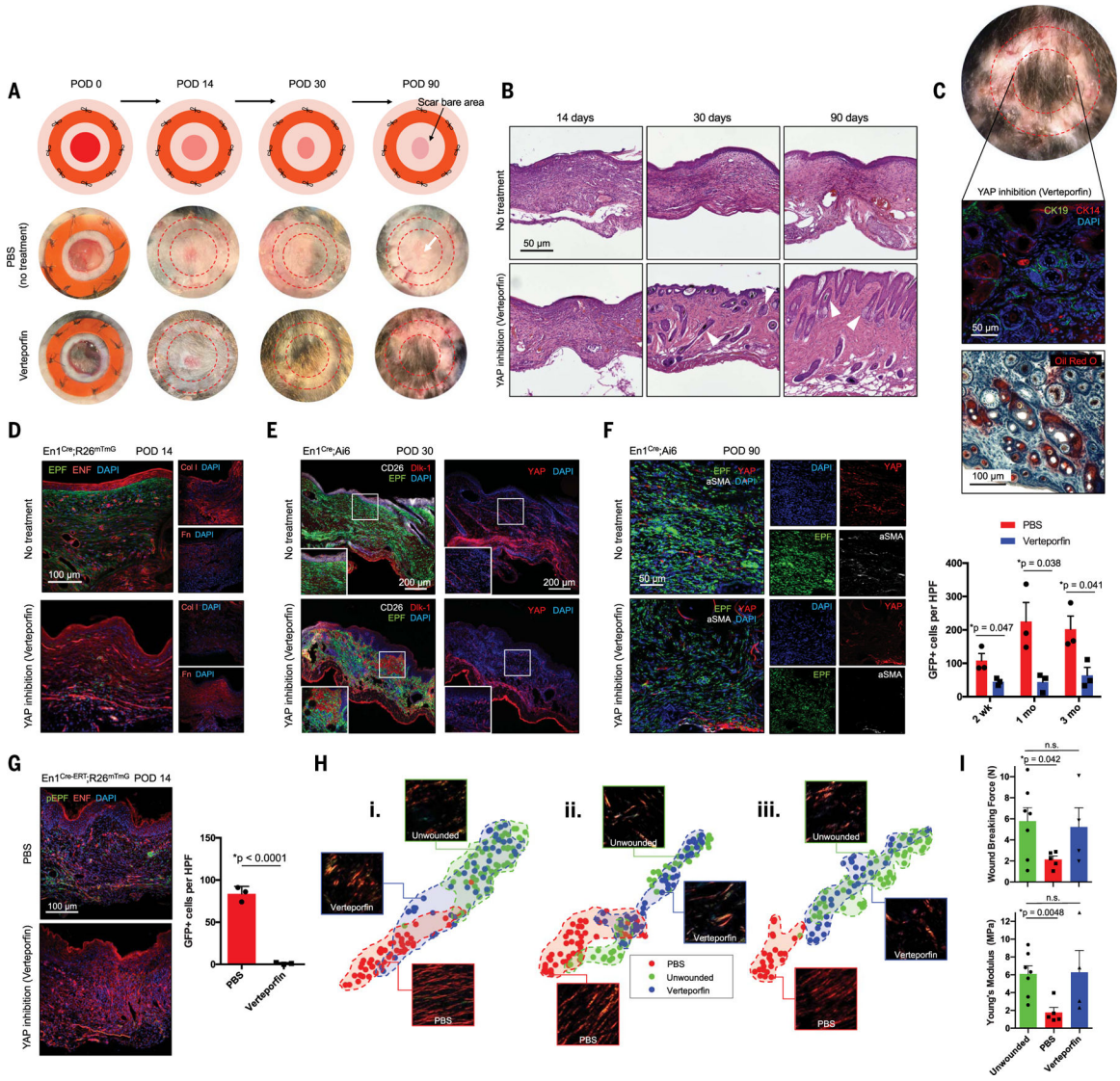

Fig. 4. Mechanotransduction inhibition in vivo results in scarless wound healing via regeneration.

(**A**) Schematic (top) and gross photographs of dorsal excisional wounds treated with PBS (control) or verteporfin. Surrounding bare area is where splint was attached and removed before harvest (red dashed circles). (**B**) H&E histology of control- and verteporfin-treated wounds. White arrowheads indicate dermal appendage–like morphology. (**C**) By POD 90, verteporfin-treated wounds regenerate HF/appendages, grossly (top) and histologically: middle, immunostaining for HF/SG markers CK14/19; bottom, Oil Red O staining (red) for SG. (**D** to **F**) Fluorescent histology of control- or verteporfin-treated wounds in indicated mice at POD 14 (D), 30 (E), and 90 (F) with immunostaining for ECM proteins (col-I, Fn) and fibroblast/mechanotransduction markers (CD26, Dlk1, YAP, α-SMA). (F) Right: EPFs per HPF in PBS- and verteporfin-treated wounds over time. (**G**) Left: Fluorescent histology of control- and verteporfin-treated *En1*$^{Cre\text{-}ERT}$;*R26*^{mTmG} wounds. Right: Quantification of pEPFs per HPF. (**H**) t-distributed stochastic neighbor embedding (t-SNE) plots visualizing ECM ultrastructural properties for skin and PBS- or verteporfin-treated wounds at POD

14 (i), 30 (ii), and 90 (iii); clusters for each condition (PBS-treated, unwounded, or verteporfin-treated) are highlighted by shaded regions. (**I**) Wound breaking force (top; unwounded versus verteporfin, $P = 0.8057$) and Young's modulus (bottom; unwounded versus verteporfin, $P = 0.9287$) calculated for unwounded skin and PBS- or verteporfin-treated wounds.

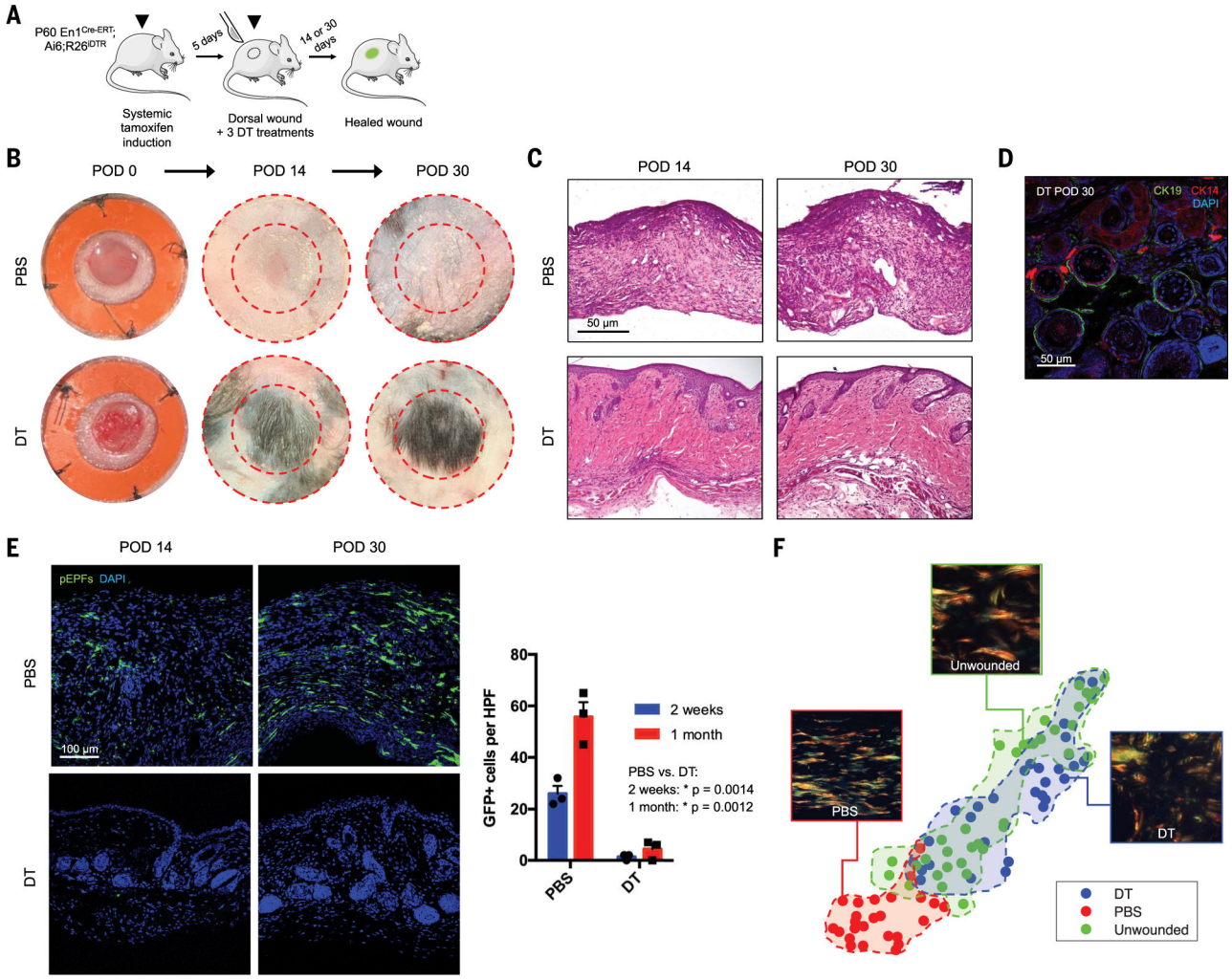

Fig. 5. Targeted ablation of *Engrailed-1*–expressing fibroblasts yields skin wound regeneration.

(**A**) Schematic of *En1*$^{Cre\text{-}ERT}$*;Ai6;R26*^{iDTR} tamoxifen induction, wounding, and diphtheria toxin (DT) treatment to ablate pEPFs generated in response to wounding. (**B** and **C**) Gross photographs (B) and H&E histology (C) of wounds treated with PBS (top) or DT (bottom) over time. (**D**) DT-treated wounds at POD 30 with immunofluorescent staining for CK14/19 (HF/SG). (**E**) Left: Fluorescent histology of PBS- and DT-treated wounds at POD 14 and 30, showing pEPFs (GFP^{+}). Right: Quantification of pEPFs per 20× HPF. (**F**) t-SNE plots visualizing 26 ECM ultrastructural properties for unwounded skin and PBS- or DT-treated wounds at POD 30; shaded regions highlight clusters of the three conditions.

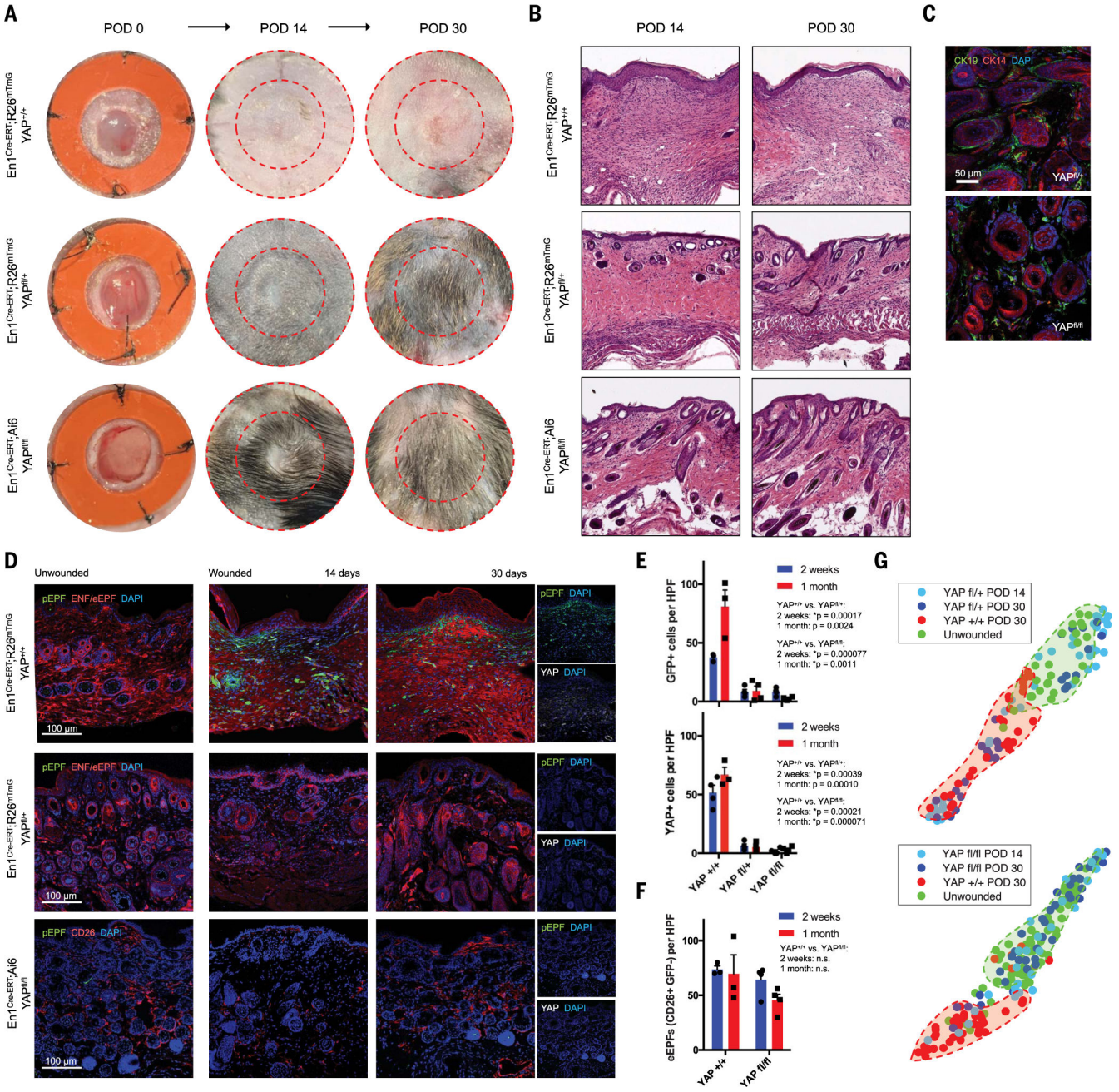

Fig. 6. YAP knockout abrogates postnatal *Engrailed-1* expression to promote skin wound regeneration.

(**A** and **B**) Gross photographs (A) and H&E histology (B) of $YAP^{+/+}$ (top), $YAP^{fl/+}$ (middle), and $YAP^{fl/fl}$ (bottom) wounds over time. (**C**) Immunofluorescent histology for CK14/19 (HF/SG) in POD 30 $YAP^{fl/+}$ (top) and $YAP^{fl/fl}$ (bottom) wounds. (**D**) Immunofluorescent histology of skin (left) and $YAP^{+/+}$ (top), $YAP^{fl/+}$ (middle), and $YAP^{fl/fl}$ (bottom) wounds at POD 14 and 30. Rightmost panels show pEPFs (GFP^+) and YAP immunostaining. (**E**) Quantification of pEPFs (top) and YAP^+ cells (bottom) per 20× HPF in $YAP^{+/+}$, $YAP^{fl/+}$, and $YAP^{fl/fl}$ wounds at POD 14 and 30. (**F**) Quantification of eEPFs ($CD26^+GFP^-$) in $YAP^{+/+}$ and $YAP^{fl/fl}$ wounds. (**G**) t-SNE plots visualizing ECM ultrastructural properties

for unwounded skin versus $YAP^{fl/+}$ (top) and $YAP^{fl/fl}$ (bottom) wounds; shaded regions highlight clusters of the four conditions.